Organic & Biomolecular Chemistry

Cite this: *Org. Biomol. Chem.*, 2012, **10**, 6693

www.rsc.org/obc

PAPER

Novel multifunctional organic semiconductor materials based on 4,8-substituted 1,5-naphthyridine: synthesis, single crystal structures, opto-electrical properties and quantum chemistry calculation†

Kun-Yan Wang,[a] Chen Chen,[a] Jin-Fang Liu,[a] Qin Wang,[a] Jin Chang,[b] Hong-Jun Zhu*[a] and Chong Li[c]

Received 14th May 2012, Accepted 20th June 2012
DOI: 10.1039/c2ob25926e

A series of 4,8-substituted 1,5-naphthyridines (**1a–1h**) have been successfully synthesised by a Suzuki cross-coupling between 4,8-dibromo-1,5-naphthyridine (**4**) and the corresponding boronic acids (**2a–2h**) in the presence of catalytic palladium acetate in yields of 41.4–75.8% and have ben well characterized. They are thermally robust with high phase transition temperatures (above 186 °C). Compounds **1b**, **1e** and **1f** crystallized in the monoclinic crystal system with the space groups $P2_1/c$, $P2_1/c$ and $P2_1/n$, respectively. All of them show the lowest energy absorption bands (λ_{max}^{Abs}: 294–320 nm), revealing low optical band gaps (2.77–3.79 eV). These materials emit blue fluorescence with λ_{max}^{Em} ranging from 434–521 nm in dilute solution in dichloromethane and 400–501 nm in the solid state. 4,8-Substituted 1,5-naphthyridines **1a–1h** have estimated electron affinities (EA) of (2.38–2.72 eV) suitable for electron-transport materials and ionization potentials (IP) of 4.85–5.04 eV facilitate excellent hole-injecting/hole-transport materials properties. Quantum chemical calculations using DFT B3LYP/6-31G* showed nearly identical the lowest unoccupied molecular orbitals (LUMO) of −2.39 to −2.19 eV and the highest occupied molecular orbitals (HOMO) of −5.33 to −6.84 eV. These results demonstrate the 4,8-substituted 1,5-naphthyridines **1a–1h** with a simple architecture might be promising blue-emitting (or blue-green-emitting) materials, electron-transport materials and hole-injecting/hole-transport materials for applications for developing high-efficiency OLEDs.

Introduction

Organic light-emitting diodes (OLEDs) have attracted considerable attention in recent decades because of their promising applications for the next generation of flat panel displays[1–3] and general lighting[4–6] with the advantages of low-driving-voltage, high-efficiency, and the possibility of flexible and large-area display applications.[7–10] Organic small molecules[11–13] have potential advantages not only in lower synthesis costs, but most importantly, organic semiconductor materials have been shown to be amenable to large scale-up, high efficiencies, and simple and inexpensive fabrication routes to realise these devices.[14–18] Maintaining a balance between electron and hole currents plays an important role in achieving high device efficiency in the field.[19] Therefore, the vast majority of synthetic effort and structure–property studies have to date been devoted to lots of organic functional materials for OLEDs.[20–23] Many nitrogen heterocyclic fused ring compounds like conjugated quinoline derivatives,[22,24–27] quinoxaline derivatives[28–33] and anthrazoline derivatives[34–37] have been investigated as building blocks for increasing the electron affinity (EA) of current electron-transport materials for OLEDs. In particular, polyquinolines and oligoquinolines exhibit outstanding electron-transport properties as a result of their high EA values.[38–40] For example, 1,5-naphthyridine is electron deficient relative to quinoline, and should have higher EA values than quinoline.[41] Until recently, only a limited number of 1,5-naphthyridine derivatives have been explored. 4-Hydroxy-1,5-naphthyridine derivatives were synthesized as chelating ligands and their metal chelates could be applied as a highly efficient non-dopant deep blue emitter, good electron-transport material and host material for yellow dopant.[42]

[a]*Department of Applied Chemistry, College of Science, Nanjing University of Technology, Jiangsu Key Laboratory of Industrial water-Conservation & Emission Reduction, Nanjing 210009, China. E-mail: zhuhjnjut@hotmail.com; Fax: +86 25 83587443; Tel: +86 25 83172358*
[b]*School of Chemistry, Physics and Mechanical Engineering, Science and Engineering Science and Engineering Faculty, Queensland University of Technology, Brisbane 4000, Australia*
[c]*Key Laboratory for Organic Electronics & Information Displays and Institute of Advanced Material, Nanjing University of Posts and Telecommunications, Wenyuan Road 9, Nanjing 210046, China*

†Electronic supplementary information (ESI) available: Experimental details and characterization data of new compounds **4**, **1a–1h**; and mass spectra of **4**, **1a–1h** and NMR spectra of **4**, **1a–1h**, calculation results of **1a–1h**, single crystal structures for **1b**, **1e** and **1f**. CCDC 866640, 881204 and 881205. For ESI and crystallographic data in CIF or other electronic format see DOI: 10.1039/c2ob25926e

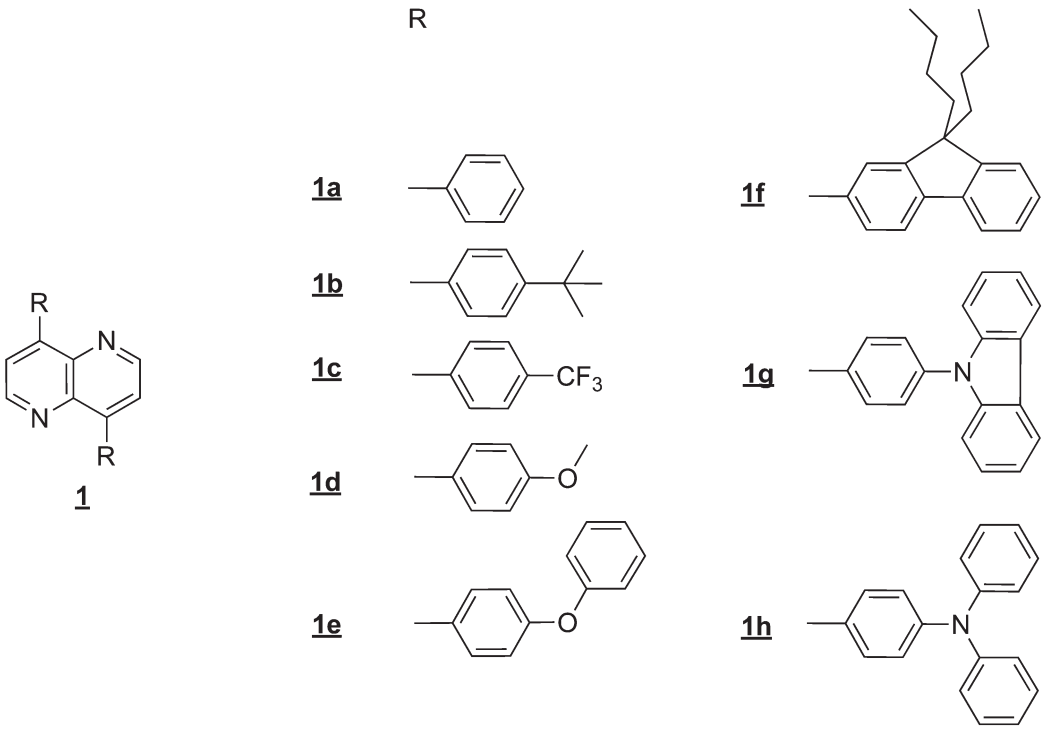

Chart 1 Structures of eight 4,8-substituted 1,5-naphthyridines **1a–1h**.

4-Diphenylphosphino-1,5-naphthyridine derivatives were also prepared as ligands for their copper(I) complexes.[43] Ru(II) complexes with 2,6-substituted and 4,8-substituted 1,5-naphthyridines as bridging ligands were investigated for their photophysical and electrochemical properties.[44] However, reports concerning the electrochemical and photophysical properties of organic small molecule materials based on 4,8-substituted 1,5-naphthyridines are limited.

Devices that have fewer layers and do not require doping are much more desirable because they simplify the fabrication process.[45–49] In this work, moieties with hole-injection/hole-transport properties, *i.e.*, triphenylamine, fluorene and carbazole were introduced into a 1,5-naphthyridine core. We aim to develop as novel hybrid materials 1,5-naphthyridines with simple architectures and to study further the underlying structure–property relationships.

In this paper, we report the synthesis, detailed structural characterization, and investigation of the electrochemical and photophysical properties of a series of eight new multifunctional materials (**1a–1h**) based on a 1,5-naphthyridine core structure with various 4,8-bisaryl groups: 4,8-diphenyl-1,5-naphthyridine (**1a**), 4,8-bis(4-(*tert*-butyl)phenyl)-1,5-naphthyridine(**1b**), 4,8-bis-(4-(trifluoromethyl)phenyl)-1,5-naphthyridine (**1c**), 4,8-bis-(4-methoxyphenyl)-1,5-naphthyridine (**1d**), 4,8-bis(4-phenoxyphenyl)-1,5-naphthyridine(**1e**), 4,8-bis(9,9-di-*n*-butyl-9*H*-fluoren-2-yl)-1,5- naphthyridine(**1f**), 4,8-bis(4-(9*H*-carbazol-9-yl)phenyl)-1,5-naphthyridine (**1g**), 4,8-bis-(4-(diphenylamino)phenyl)-1,5-naphthyridine (**1h**) (Chart 1). These materials show superior properties including high relatively fluorescence quantum efficiency for **1g** and **1h**, excellent thermal stabilities, suitable lowest unoccupied molecular orbital (LUMO) similar to oligoquinolines and proximate highest occupied molecular orbital (HOMO) close to the work function of indium tin oxide (ITO), which could make them possible candidates for a class of blue-emitting (or blue-green-emitting) materials, electron-transport materials and hole-injecting/hole-transport materials in OLEDs.

Results and discussion

2.1. Synthesis and characterization

Scheme 1 outlines the synthesis of the series of blue fluorescent materials 4,8-substituted 1,5-naphthyridines. The detailed procedures for the synthesis of the reaction intermediates and final products are described in the ESI.† The synthesis procedures of molecules **1a–1h** contain three parts: synthesis of the arms (aryl boronic acids **2a–2h**) (Scheme 2), synthesis of the key intermediate 4,8-dibromo-1,5-naphthyridine **4** (Scheme 3) and Pd-catalyzed Suzuki coupling reactions of compound **4** with **2a–2h**. Suzuki coupling reactions in the synthetic route to **1a–1h** were catalyzed by $Pd(OAc)_2$ in mixed solvent (*N*,*N*-dimethylformamide, DMF–H_2O), giving the desired products **1a–1h**, respectively, in 41.4–75.8% yields. Compounds **1a** and **1c** were obtained as white powders, and **1b** was obtained as small colorless crystals, **1d**, **1e** and **1f** as light yellow needles, **1g** as a light yellow powder and **1h** as a bright yellow powder. All these newly synthesized 4,8-substituted 1,5-naphthyridines (**1a–1h**) were purified by recrystallization with methanol and THF twice and fully characterized by ^1H and ^{13}C NMR spectroscopy, IR spectroscopy and mass spectrometry (MS) (shown in Fig. S21–S44 in ESI†). The purity of 1,5-naphthyridines **1a–1h** was also confirmed by elemental analysis with satisfactory results. All these spectra confirmed the proposed structures

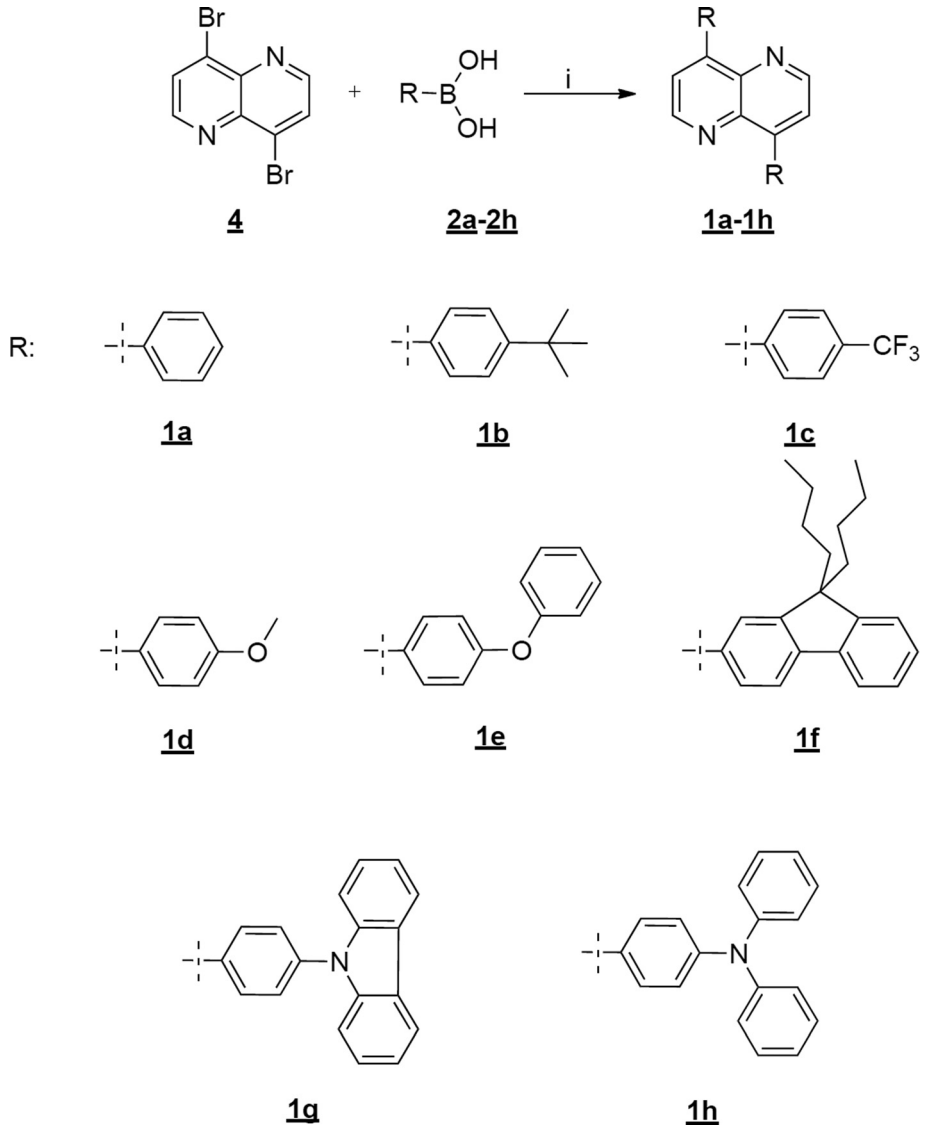

Scheme 1 Synthesis of 4,8-substituted 1,5-naphthyridines **1a–1h** by a Suzuki coupling reaction. Reagents and conditions: (i) $Pd(AcO)_2$, K_2CO_3, DMF + H_2O, 80 °C.

of 1,5-naphthyridines **1a–1h**. The solubility of the products is good in many common solvents, *e.g.* THF, toluene, chloroform, and dichloromethane (DCM), therefore they offer the possibility of solution processing, such as ink jet printing and roll-to-roll processing, a prerequisite for large area applications.[50]

Briefly, compound **4** (shown in Fig. S18–S20 in ESI†) was prepared as a key intermediate in a yield of 79.3% by bromination with $POBr_3$ from 1,5-naphthyridine-4,8(1*H*,5*H*)-dione (**3**), whose synthetic route was described in Scheme 3 according to Brown and Dewar.[51] Besides, the aryl boronic acid arms **2a–2h** were also very important for the synthesis of materials **1a–1h**, which were prepared *via* Grignard reaction[52] of **3a–3e** and by lithiation[53] of **3f–3h** in good yield of 59.5%–93.3%, followed by treatment with trimethyl borate and hydrolysis catalyzed by acid. The synthetic routes to intermediates **3e–3h** are shown in Scheme 4 according to the corresponding literature.[54–57]

2.2. Thermal properties

The thermal properties of 4,8-substituted 1,5-naphthyridines **1a–1h** were investigated by differential scanning calorimetry (DSC) analyses, shown in Table 2 (see below). DSC was used to investigate phase transitions (**1a–1h** are shown in Fig. S1 in ESI†). No glass transitions or crystallization events were observed by DSC scans of any of the molecules except for **1b** (glass transition temperature, T_g = 247 °C) and **1g** (T_g = 221 °C). These eight 1,5-naphthyridine-based materials are thermally stable and lack any detectable phase transitions at low temperatures, indicating they are suitable for OLED fabrication. All the materials had melting transitions ranging from 186 °C for **1f** to 365 °C for **1g**. As might be expected, the compound **1f** containing hexyl group has the lowest melting temperature of 186 °C, and **1g** has the highest melting temperature of 367 °C because of the great planar rigidity of the 4-(9*H*-carbazol-9-yl)-

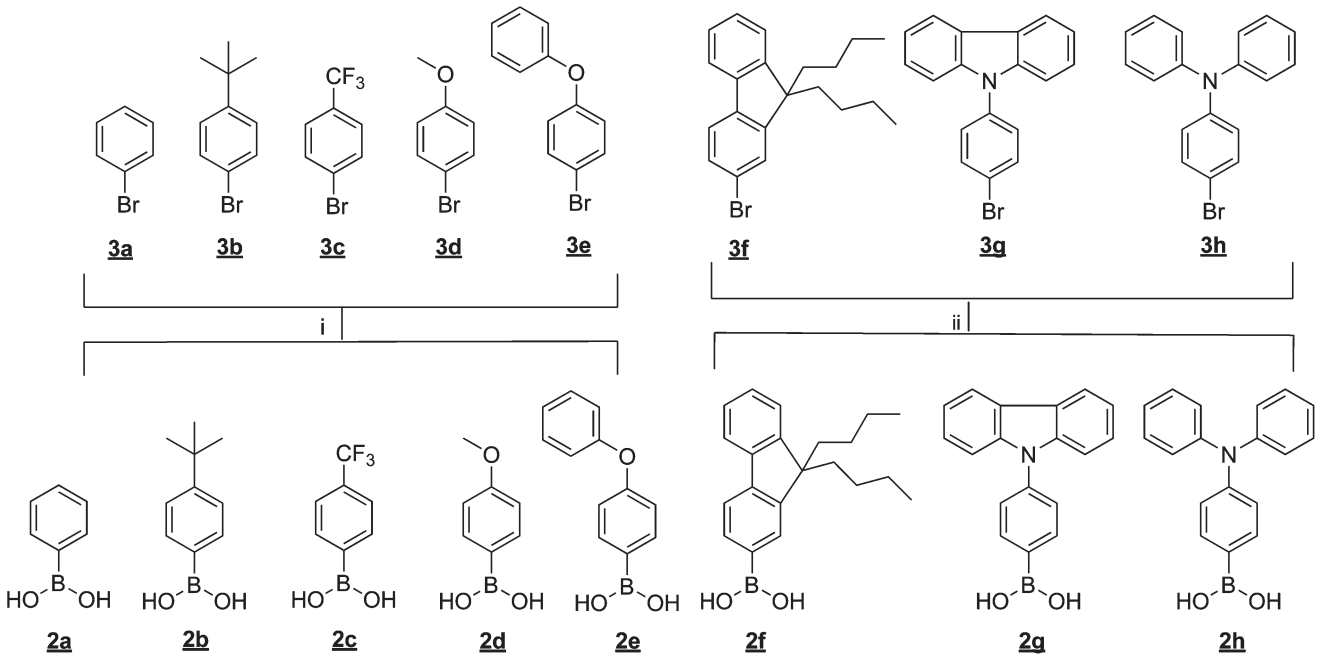

Scheme 2 Synthesis route to aryl boronic acid arms (**2a–2h**). Reagents and conditions: (i) $^{(1)}$Mg, THF, $^{(2)}B(OCH_3)_3$, −30 °C, $^{(3)}H_3O^+$; (ii) $^{(1)}n$-BuLi, THF, −78 °C, $^{(2)}B(OCH_3)_3$, −78 °C, $^{(3)}H_3O^+$.

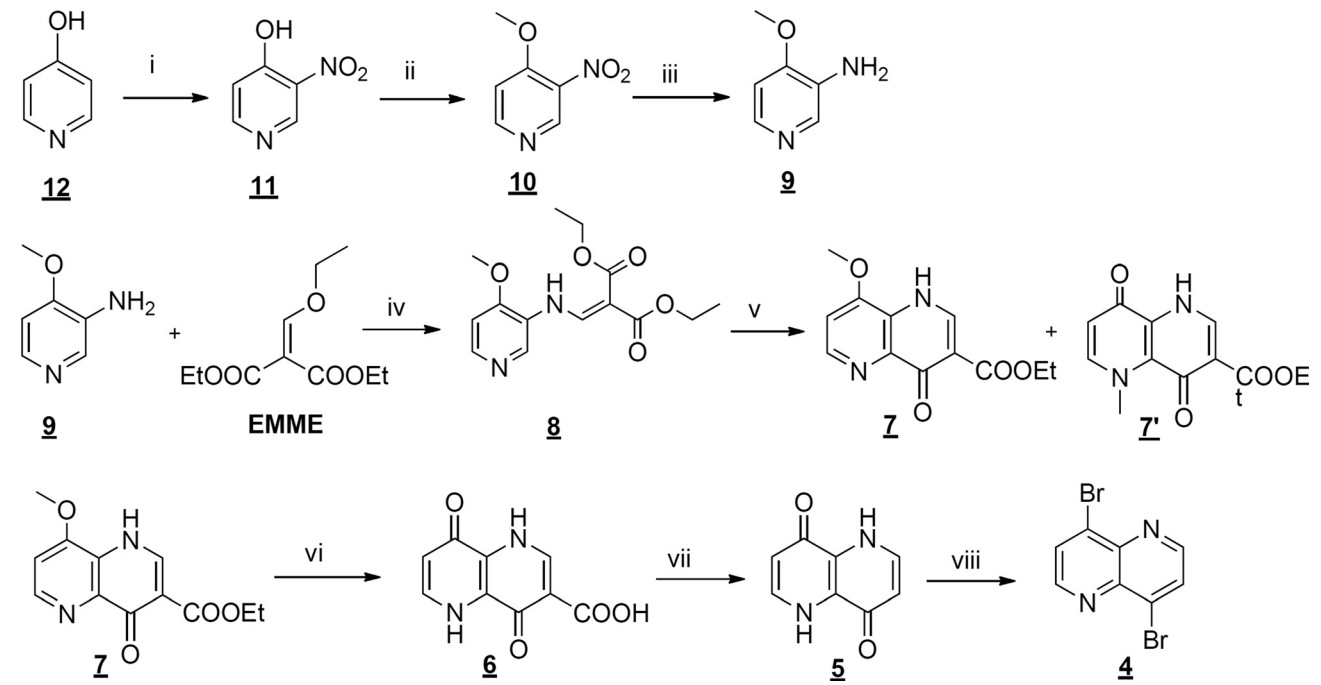

Scheme 3 Synthesis route to the key intermediate 4,8-dibromo-1,5-naphthyridine (**4**). Reagents and conditions: (i) concentrated sulfuric acid, KNO_3, 0 °C; (ii) $NaOCH_3$, CH_3OH, 0 °C; (iii) Fe, HCl, CH_3OH–H_2O; (iv) toluene, reflux; (v) diphenyl ether, reflux, 25 min; (vi) concentrated hydrobromic acid, reflux; (vii) quinoline, reflux;[51] (viii) $POBr_3$, CH_3CN.

phenyl group. These data reveal that materials **1a–1h** possess excellent thermal stability. High thermal stability is advantageous for OLED applications, as it enhances device stability and lifetime.

2.3. X-ray crystal structures of compounds 1b, 1e and 1f

Crystals were grown by slow evaporation of dichloromethane–hexane, THF–hexane, and THF–methanol solutions for

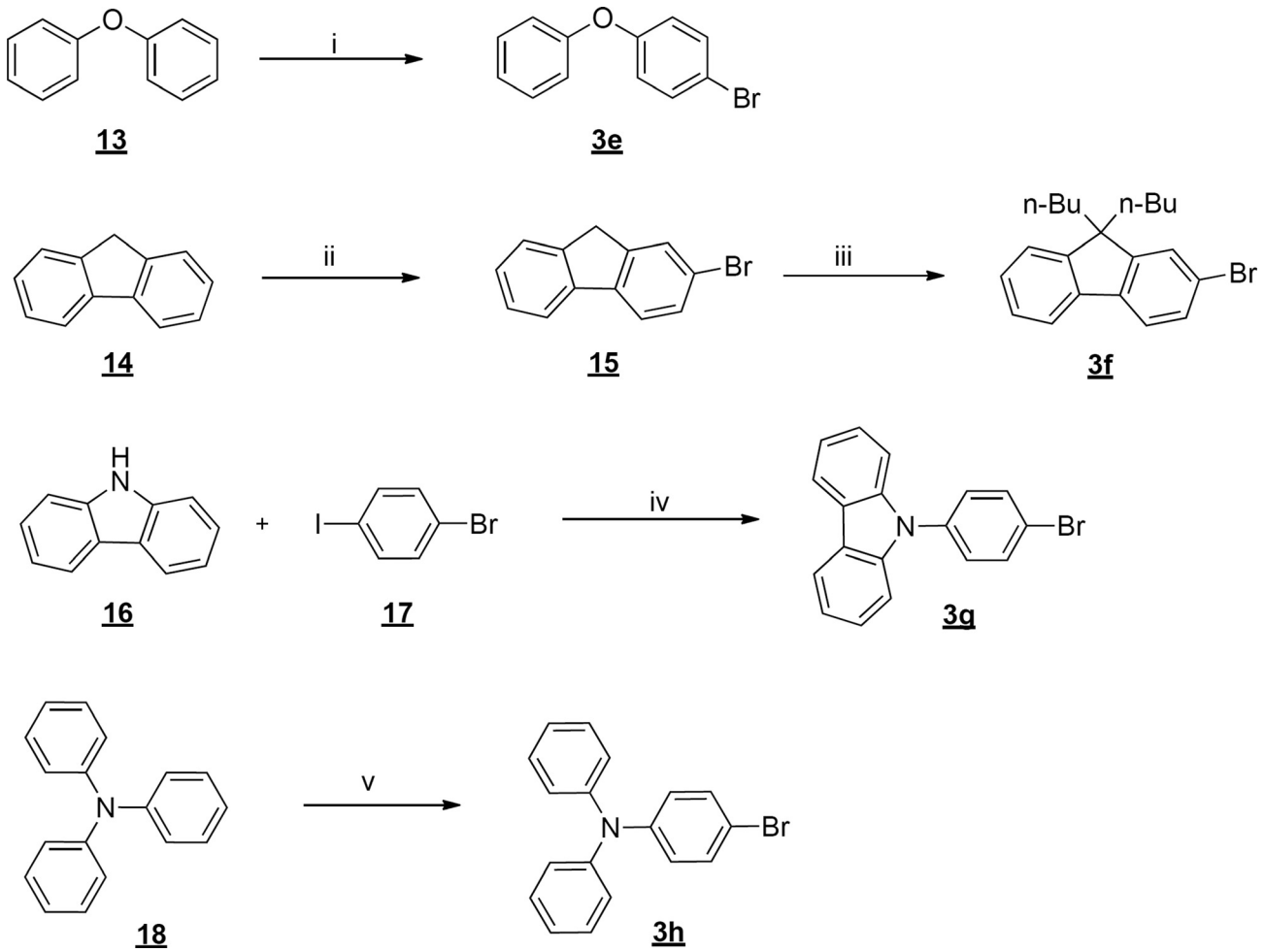

Scheme 4 Synthesis route to other intermediates. Reagents and conditions: (i) NBS, NH_4NO_3, CH_3CN, 25 °C, 30 min;[57] (ii) NBS, propylene carbonate, 60 °C; (iii) *n*-butyl bromide, KOH, KI, DMSO, 60 °C;[75] (iv) CuI, DMF, K_2CO_3, reflux;[55] (v) NBS, DMF, 25 °C.[54]

compounds **1b**, **1e** and **1f**, respectively. The diffraction data were collected on a Nonius CAD4 single crystal diffractometer equipped with a graphite-monochromated MoKa radiation (λ = 0.71073 Å) by using an $\omega/2\theta$ scan mode at 293 K. The crystal structures were solved by direct methods and refined by the full-matrix least squares procedure on F^2 using SHELXL-97.[58] All nonhydrogen atoms were refined anisotropically, and the hydrogen atoms were introduced at calculated positions. Single crystals from three of the eight 1,5-naphthyridines (**1b**, **1e** and **1f**) were suitable for the determination of X-ray crystal structures. **1b** was obtained as thin colorless prisms, and **1e** was obtained as yellow blocks. Colorless needles were obtained for **1f** resulting in excellent quality data. **1b** and **1e** were found to have primitive monoclinic crystal systems. The unit cell parameters of a = 11.973(2) Å, b = 7.8020(16) Å, c = 12.534(3) Å and β = 102.95(3)° for **1b**, a = 9.869(2) Å, b = 14.785(3) Å, c = 16.173(3) Å and β = 95.51(3)° for **1e**, and a = 8.9420(18) Å, b = 10.249(2) (16) Å, c = 21.626(4) Å and β = 96.87(3)° for **1f** are reported for the molecules. The space groups were $P2_1/c$, $P2_1/c$ and $P2_1/n$ for **1b**, **1e**, and **1f**, respectively. Structures were refined to final residuals of R_1 = 7.59% for **1b**, R_1 = 7.56% for **1e**, and R_1 = 7.66% for **1f**. The detailed crystallographic data for **1b**, **1e** and **1f** are collected in Table 1.

The single crystal structures and some packing diagrams of **1b**, **1e** and **1f** are shown in Fig. 1–3 (other packing diagrams of **1b**, **1e** and **1f** are shown in Fig. S45–S47 in ESI†). The core 1,5-naphthyridine is almost coplanar for these three compounds. The 4-(*tert*-butyl)phenyl groups are twisted 46.7° from the plane of the 1,5-naphthyridine unit in **1b**. The crystal structure of **1e** is a double molecular structure. Its structural unit consists of two similar **1e** molecules. The two α-linked phenyl groups are twisted 40.3° and 42.4° from the plane of the 1,5-naphthyridine unit in **1e**. The dihedral angles of the two phenyl moieties in the 4-phenoxyphenyl groups are 69.6° and 70.9° for **1e**. The α-linked phenyl group in **1f** is twisted 40.7° from the core plane. This suggests that the planarity of the molecules could increase with longer 4,8-substituents and also demonstrates that a *tert*-butyl substituent might be beneficial to achieve more bulky molecules and alter the conjugation by means of its steric hindrance. Crystal **1b** exhibits edge-to-face packing of the substituted phenyl rings to neighboring planar core units (1,5-naphthyridines and the bis(α-linked phenyl) groups). In the molecular packing of **1e**, offset face-to-face π-stacking interactions between neighboring molecular 1,5-naphthyridine units are observed and the intermolecular distance is 3.94 Å. Additionally **1e** has edge-to-face packing of α-linked benzene rings in the

4-phenoxyphenyls of neighboring molecules with distances of 2.92–2.97 Å. The other benzene rings of the 4-phenoxyphenyls in neighboring molecules also exhibit edge-to-face packing with distances of 2.94–3.02 Å. However, no π-stacking interaction is observed in crystal **1f** because the *n*-butyl groups could expand the distance of neighboring molecules. This indicates that **1f** has very weak intermolecular interactions. As a result, the maximum emissions of **1f** are the same at 435 nm both in dichloromethane and in the solid state.

2.4. Optical properties

The absorption spectra of all eight 1,5-naphthyridines in dilute dichloromethane solution (5×10^{-5} M) are shown in Fig. 4. Photoluminescence spectra both in dilute dichloromethane solution (10^{-6} M) (a) and in the solid state (b) are shown in Fig. 5. Table 2 lists their optical properties.

The solution absorption spectra of unsubstituted **1a**, alkyl substituted **1b** and **1c**, alkoxyl substituted **1d** and phenoxyl substituted **1e** show absorption maxima (λ_{max}^{Abs}) ranging from 294 to 320 nm, which corresponds to n–π* absorption from their parent 1,5-naphthyridine according to Singh.[44] As expected, the λ_{max}^{Abs} of *tert*-butyl substituted **1b**, methoxyl substituted **1d** and phenoxyl substituted **1e** are red-shifted by 6 nm, 18 nm and 15 nm compared with unsubstituted **1a** owing to the electron-donating *tert*-butyl, methoxyl and phenoxyl moiety respectively. The absorption λ_{max}^{Abs} of trifluoromethyl substituted **1c** is blue shifted by 8 nm compared with **1a** as a result of the electron attracting effect of the trifluoromethyl group. Fluorene containing **1f**, 9*H*-carbazol-9-yl substituted **1g** and diphenylamino substituted **1h** have absorption λ_{max}^{Abs} that are red-shifted 41 nm, 40 nm and 97 nm respectively compared with **1a** as these substituents could extend the conjugated backbone and increase electron density. The diphenylamine derivative (**1h**) possesses the longest wavelength absorption while the carbazole derivative (**1g**) shows a shorter wavelength absorption compared with **1h**.

Table 1 Crystallographic data for 4,8-substituted 1,5-naphthyridines **1b**, **1e** and **1f**

	1b	**1e**	**1f**
Formula	$C_{28}H_{30}N_2$	$C_{32}H_{22}N_2O_2$	$C_{50}H_{54}N_2$
Formula weight	394.55	466.52	682.98
Crystal system	Monoclinic	Monoclinic	Monoclinic
Color of crystal	Colorless	Orange	Colorless
Space group	$P2_1/c$	$P2_1/c$	$P2_1/n$
a [Å]	11.973(2)	9.869(2)	8.9420(18)
b [Å]	7.8020(16)	14.785(3)	10.249(2)
c [Å]	12.534(3)	16.173(3)	21.626(4)
β (°)	102.95(3)	95.51(3)	96.87(3)
Volume [Å^3]	1141.1(4)	2348.9(8)	1967.7(7)
Temperature [K]	293(2)	293(2)	293(2)
Z	4	4	4
F(000)	424	976	736
$D_{calcd.}$ (g cm^{-3})	1.148	1.319	1.153
μ (Mo-Kα)(mm^{-1})	0.067	0.083	0.066
R_{int}	0.0861	0.0424	0.0396
No of reflection	2101	4310	3607
No of parameters	124	325	235
R_1, R_1	0.0759, 0.1810	0.0756, 0.1729	0.0766, 0.1535
wR_2, wR_2	0.1069, 0.1340	0.1411, 0.1725	0.1626, 0.1974
GOF	1.002	1.004	1.005

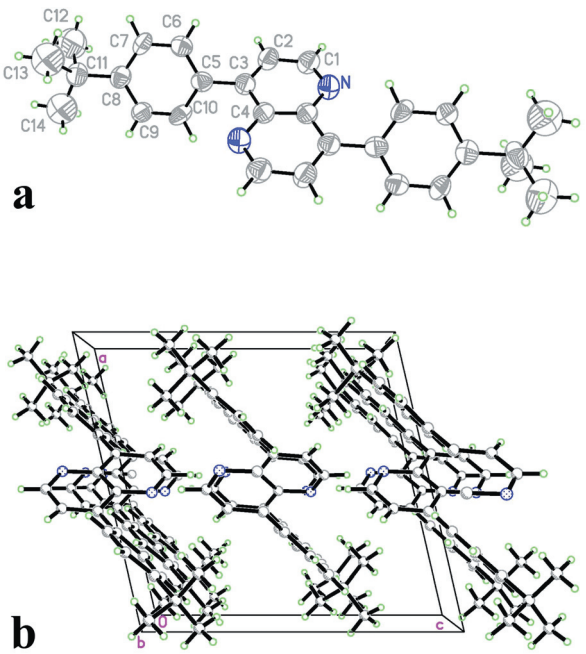

Fig. 1 Single crystal structure of **1b** (a), view down the *b* axis (b).

Table 2 Photophysical properties of 4,8-substituted 1,5-naphthyridines **1a–1h**

Compd.	Thermal T_g/T_m (°C)	$\varepsilon \times 10^4$ (M^{-1} cm^{-1})	Photophysical					
			λ_{abs} [a] (nm)	λ_{edge} (nm)	E_g^{opt} [b] (eV)	E_g^{cal} [c] (eV)	λ_{em} [d,e] (nm)	Φ_u [f]
1a	—/270	2.37	302	333	3.72	4.22	448 (403)	0.06
1b	247/300	2.23	308	347	3.57	4.08	441 (401)	0.03
1c	—/268	2.62	294	327	3.79	4.32	443 (400)	<0.005
1d	—/253	2.39	320	378	3.28	3.89	434 (423)	0.09
1e	—/210	1.84	317	367	3.38	3.91	439 (421)	0.19
1f	—/186	2.84, 2.75	275, 343	391	3.17	3.63	435 (435)	0.14
1g	221/365	5.27, 2.97	293, 342	397	3.12	3.36	479 (445)	0.61
1h	—/280	3.71, 2.43	302, 399	448	2.77	3.09	521 (501)	0.80

[a] Recorded in 5×10^{-5} M solutions of dichloromethane at r.t. [b] Optical band gaps determined from the absorption edge of the normalized absorption spectra. [c] Optimized using density functional theory (DFT) methods at the B3LYP/6-31G* level. [d] Recorded in 10^{-6} M solutions of dichloromethane at rt. $\lambda_{excitation} = \lambda_{abs}$ of the lower energy band ($\lambda_{excitation}^{solid}$ = 300 nm for **1a** to **1g**, 400 nm for **1h**). [e] Values in parentheses correspond to fluorescence in solid state. [f] Quantum yield (Φ_u) measured in dilute dichloromethane relative to that of 9,10-diphenyl anthracene (0.9 in cyclohexane). Excitation wavelength = 320 nm for **1a** to **1f**, 365 nm for **1g** and **1h**.

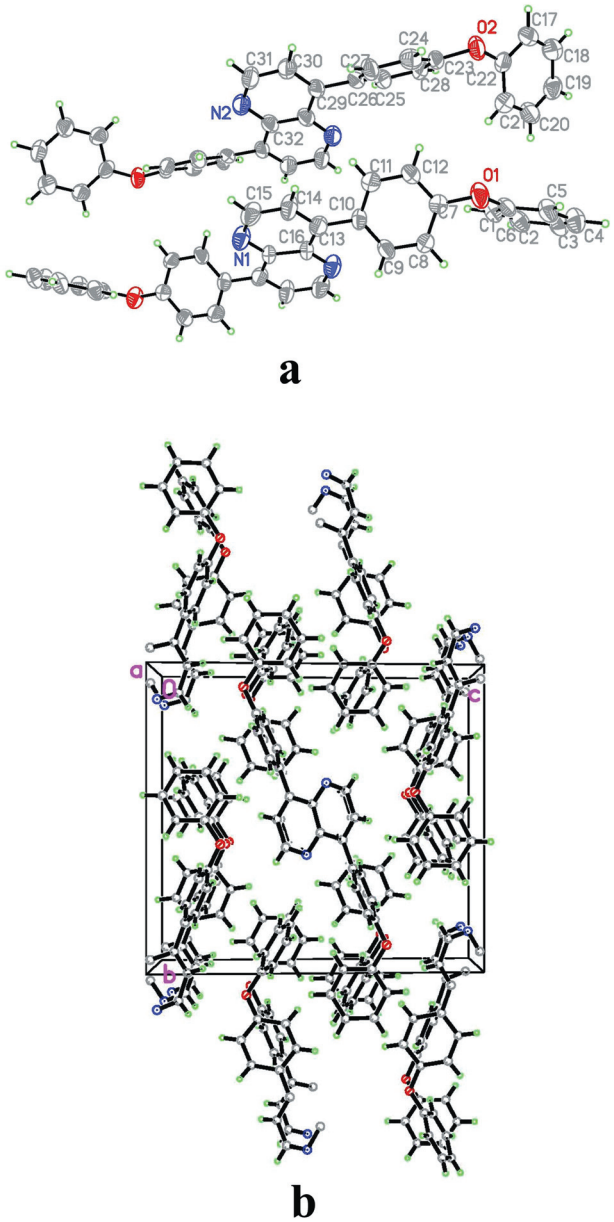

Fig. 2 Single crystal structure of **1e** (a), view down the *a* axis (b).

The extended conjugation present in the above derivatives may lead to a red-shifted absorption. On the contrary, the blue-shifted profile observed for **1g** may be attributed to the retardation of electronic delocalization caused by the twist between the carbazole and α-linked phenyl group (*vide supra*).[59] Optical band gaps (E_g^{opt}) determined from the absorption edge are given in Table 2 and vary from 2.77 eV for **1h** to 3.79 eV for **1c**, slightly bigger than for 4,8-diphenyl-1,5-anthrazolines.[34,37] Compound **1h** has the lowest bandgap of 2.77 eV, which is attributed to better π-conjugation of the 4-(diphenylamino)phenyl substituent over other substituted derivatives.

Each absorption spectrum of compound **1f**, **1g** and **1h** shows two main absorption peaks, in which the higher energy bands are at 275 nm, 293 nm and 302 nm, respectively and the lower energy bands at 343 nm, 342 nm and 399 nm. The higher energy bands may be from the π–π* or n–π* transitions of the fluorene moiety, 9-phenyl-9*H*-carbazole moiety and triphenylamine moiety by virtue of the large molar extinction coefficients (ε > 28 400 M^{-1} cm^{-1}), shown in Table 2. The lower energy bands in the region of 342 nm to 399 nm probably originate from the charge transfer transition between the electron rich substituent groups and electron accepting 1,5-naphthyridine core.[60–62] The mediocre intensity observed for the charge transfer transition indicates a poor orbital overlap. Such weak charge transfer transitions are also reported for indoloquinoxaline derivative hybrid materials.[60]

The dilute solution photoluminescence (PL) spectra (Fig. 5a) of **1a–1h** show that compounds **1a–1g** in dilute solution in dichloromethane emit blue light with the emission maximum ranging from 434 nm for **1d** to 479 nm for **1g** while compound **1h** emits blue-green light at 521 nm because of its long conjugation length. The blue shift for 9*H*-carbazol-9-yl substituted **1g** compared with diphenylamine derivative **1h** is also observed in aryl-oxadiazole–fluorene triad molecules.[63]

The PL quantum yield (Φ_u) of compounds **1a–1h** in dilute solution in dichloromethane ranged from 0.03 for **1b** to 0.80 for **1h** (Table 2) whereas that of **1c** is significantly lower (<0.005). The PL quantum yields measured in dilute dichloromethane solution using 9,10-diphenylanthracene (Φ_u = 0.9) as standard increase with the increase of substituted aromatic ring electron density. The lower emission quantum yield in **1c** is due in large part to the donor–acceptor–donor nature of this 1,5-naphthyridine and weak intramolecular charge transfer for the substituted 4-(trifluoromethyl)phenyl group.[64] On the contrary, carbazole derivative **1g** and diphenylamine derivative **1h** had dramatically high quantum yields, presumably due to significant intramolecular charge-transfer (ICT) attributed to the strongly electron-donating carbazole and diphenylamine respectively.[65]

Compounds **1a–1g** emit in the blue region (Fig. 5b) with the emission peaks in the range of 400–445 nm in the solid state while **1h** emits in the blue-green region with an emission peak at 501 nm. The main absorption bands observed in solution are also seen in the solid state. The solid state absorption bands are, however, blue shifted in 1,5-naphthyridine compounds except for **1f** compared with their corresponding ones in solution. **1f** has the same maximum emission wavelength both in solution and in solid state owing to the space effect of long *n*-butyl in fluorene moiety. The order of λ_{Em} of the eight 1,5-naphthyridines in the solid state agrees with their λ_{Abs} in solution.

The absorption and fluorescence emission spectra of **1g** in various solvents are shown in Fig. 6 while the absorption and fluorescence emission spectra of the other compounds are shown in the ESI (Fig. S2–S17†). The absorption and fluorescence emission spectral data are listed in Table 3. All of the 1,5-naphthyridines studied in this work exhibited a slight shift in the absorption peak when recorded in different polar solvents such as toluene, dichloromethane, THF, acetonitrile and dimethylformamide (shown in Fig. S2–S9†). This reveals that the absorption maxima of 1,5-naphthyridines are almost independent of solvents. However, in solution, compounds **1g** and **1h** show a strongly solvent-dependent emission band while the shifts of the other compounds' emission maxima with solvents are not obvious. The fluorescence emission spectra of the two compounds shift toward longer wavelength with increasing polarity of the solvents. This might be due to the difference in

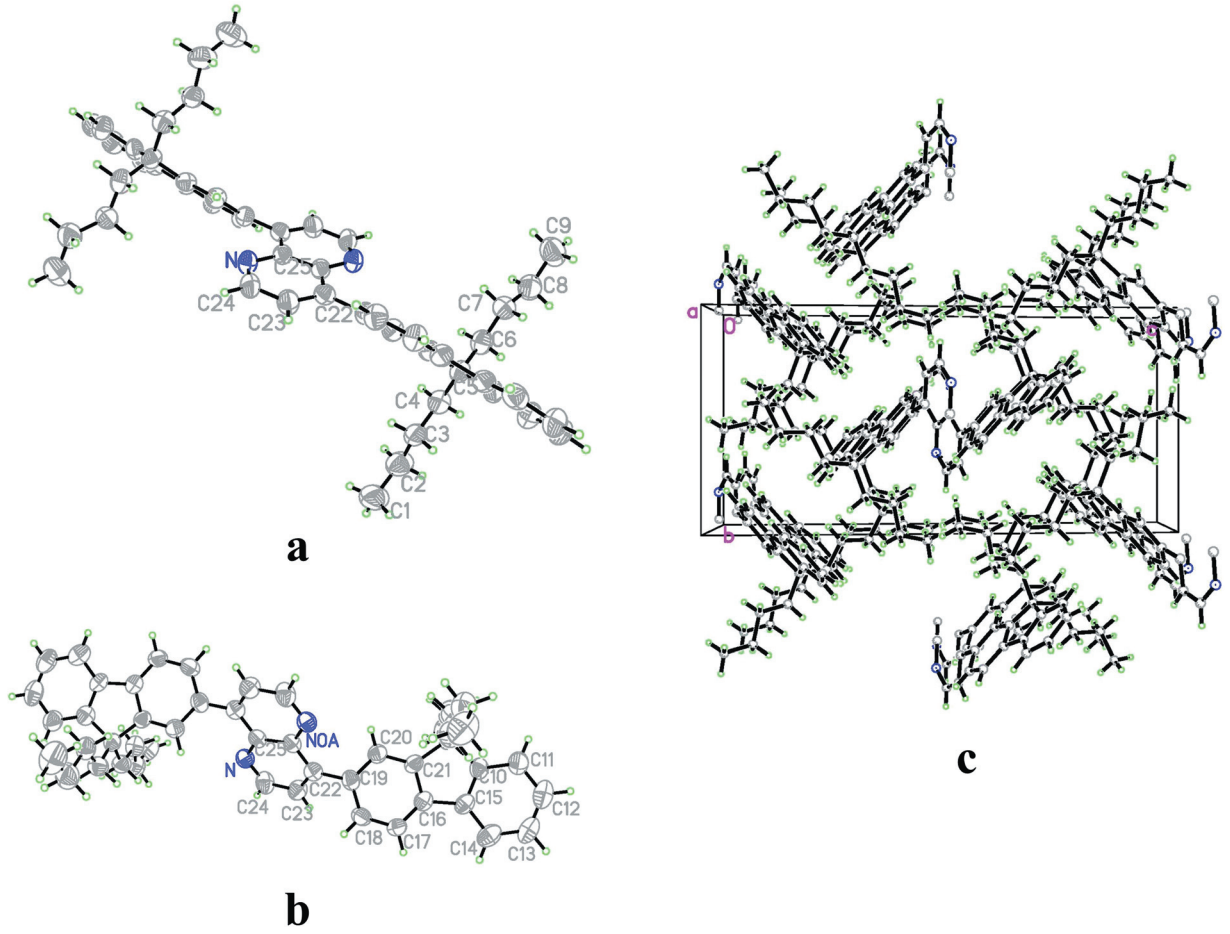

Fig. 3 Single crystal structure of **1f** (a), (b), view down the *a* axis (c).

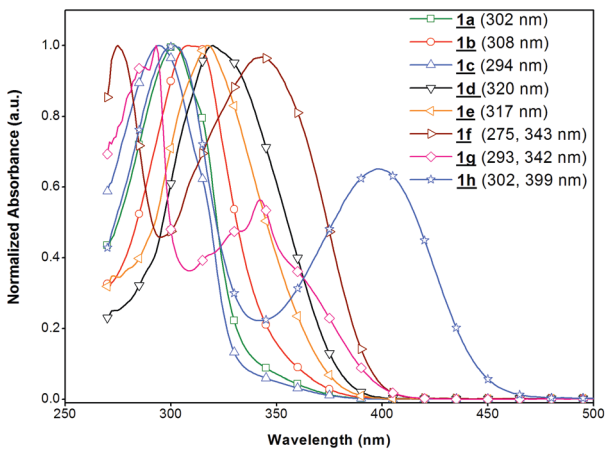

Fig. 4 UV-vis absorption spectra of **1a–1h** in DCM solution (5×10^{-5} mol L^{-1}).

the dipole moments of the molecules in the ground state and the excited states and their stabilization by solvent molecules involving various specific interactions such as dipole–dipole, hydrogen bonding, and solvation.[59] Compounds **1g** and **1h** are confirmed to be bipolar molecules and therefore could have potential applications as multifunctional organic semiconductor materials.

2.5 Electrochemical properties

The electrochemical behavior of the eight materials **1a–1h** in dichloromethane–acetonitrile (7 : 3 v/v) solution has been examined by the reduction cyclic voltammograms (CVs) using a standard one-compartment three-electrode cell equipped with a platinum disk as working electrode, a Ag/Ag^+ electrode (Ag in 0.1 M $AgNO_3$ solution, from CHI, Inc.) as the reference electrode, a Pt wire as the auxiliary electrode, and tetrabutylammonium perchlorate, TBAP (0.1 M), dissolved in dichloromethane–acetonitrile (7 : 3 v/v) as an electrolyte solution.

The cyclic voltammograms (CVs) of materials **1a** and **1h** using ferrocene as a standard are shown in Table 4 while the CVs of the other compounds are shown in the ESI (Table S1†). All eight compounds in solution clearly show oxidation peaks (0.74 V to 0.89 V *vs.* SCE) and reduction peaks (−2.23 V to −2.01 V *vs.* SCE). These suggest both hole and electron transport leading to a single-layer electroluminescent device.

Table 5 shows the solution electrochemical data for **1a–1h**. Reduction potentials vary from −2.01 V for **1c** to −2.23 V for **1f** (*vs*. SCE) and the onset reduction potentials of **1a–1h** are in the range of −1.68 to −2.02 V (*vs.* SCE). Electron affinities (EA) were estimated from the onset reduction potentials in the solution CVs ($EA = E_{red}^{onset} + 4.4$ eV) under the premise that the energy level of SCE is 4.4 eV below the vacuum level.[37] These compounds have EA values of 2.38–2.72 eV (below vacuum), in

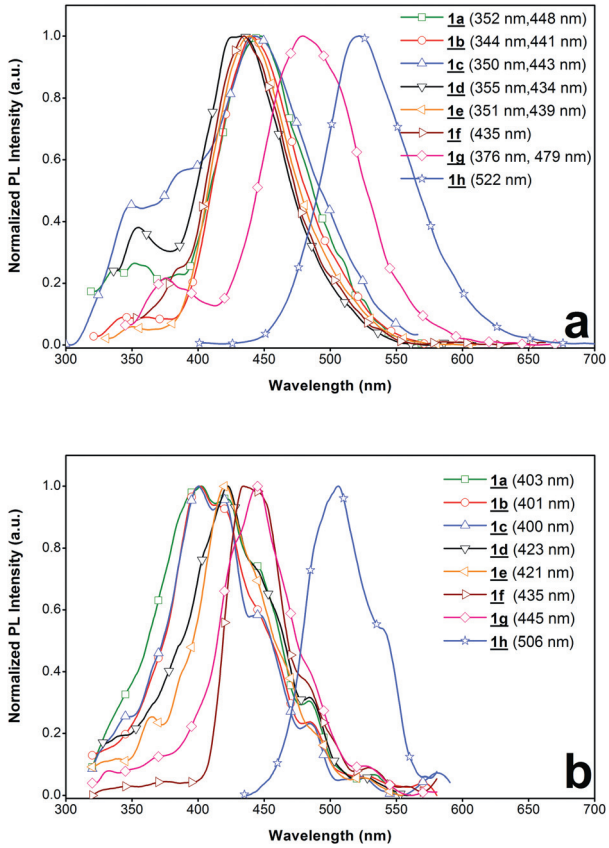

Fig. 5 PL spectra of **1a–1h** in DCM solution (~10^{-6} mol L^{-1}) (a) and in the solid state (b).

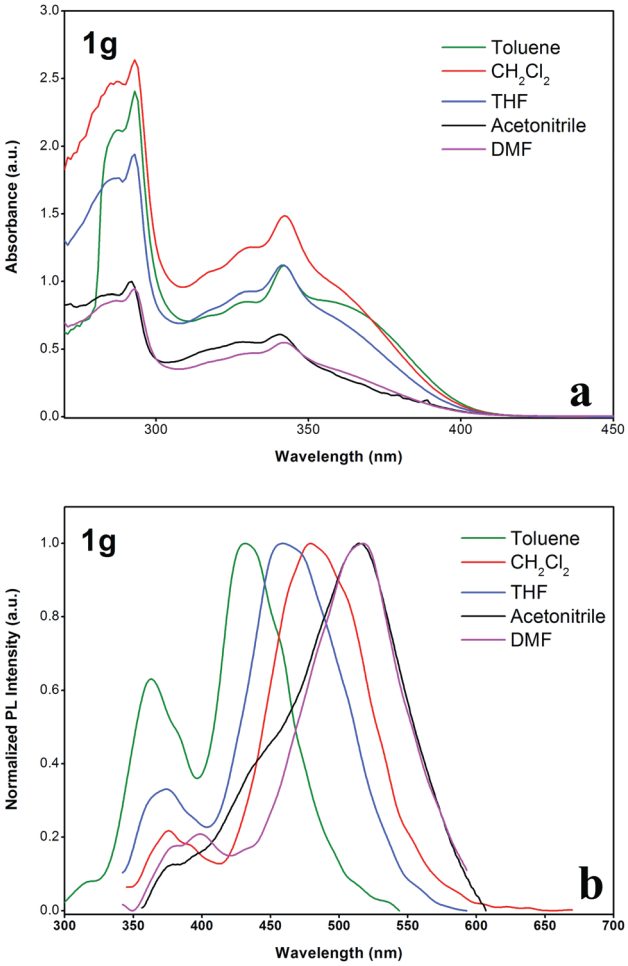

Fig. 6 UV-vis absorption spectra (a) and fluorescence emission spectra (b) of **1g** in different solvents.

which material **1g** has the highest EA values of 2.72 eV. The EA values of these 1,5-naphthyridines are similar to the EA values of oligoquinolines[66,67] and polyquinolines[68–70] already found to be good electron-transport materials for OLEDs. This suggests that these 1,5-naphthyridines could be attractive because of their excellent electron-transport materials properties.

Compounds **1a** and **1c** have one irreversible oxidation peak. In the case of compounds **1b** and **1d–1g**, two or more irreversible oxidation peaks were seen in their CVs. Oxidation cyclic voltammograms of compound **1h** having two terminal triarylamine moieties showed that starting from the second cycle an additional peak developed at a potential lower than the oxidation of the starting compounds (Fig. 7) also observed in CVs of triphenylamine–oxadiazole–fluorene triad molecules.[71] This might be due to electropolymerisation of triarylamine derivative **1h** and deposition of the polymer on the electrode surface. The formal oxidation potential varies from 0.74 V for **1h** to 0.89 V for **1c** (*vs.* SCE) and the onset oxidation potentials of **1a–1h** are in the range 0.49 to 0.64 V (*vs.* SCE). Ionization potentials (IP) were estimated from the onset oxidation potentials in the solution CVs (IP = E_{ox}^{onset} + 4.4 eV) by using the ferrocene energy level of 4.4 eV *versus* vacuum. These compounds had IP values of 4.89–5.04 eV (below vacuum) which are close to the work function of ITO and thus this allows efficient hole injection from the ITO.[72–74] Therefore 1,5-naphthyridines **1a–1h** might be candidates for excellent hole-injecting/hole-transport materials for OLEDs.

2.6 Theoretical calculation

The geometry of the highest occupied molecular orbital (HOMO) and the lowest unoccupied molecular orbital (LUMO) energy levels of **1a–1h** were optimized using density functional theory (DFT) method at the B3LYP/6-31G* level, as implemented in the Gaussian 09 program. The core 1,5-naphthyridine moiety shows a nearly coplanar structure, while the arm substituents on the 1,5-naphthyridine unit (R group) are twisted from the plane of the core. This geometry could lead to excellent solution processability. From the density distribution, it is clear that for the molecules the HOMO distributes in the whole molecule for **1a–1f** with slightly higher density on the 1,5-naphthyridine core units, which is very beneficial to hole transport through the molecules when used as hole-injecting/hole-transporting materials in OLEDs. The HOMO orbitals of compounds **1g–1h** are located mainly on the two arms of the molecule. The HOMO energy values of **1a–1h** were from −6.84 to −5.33 eV, respectively. The LUMO orbitals are predominantly located on the 1,5-naphthyridine core units for materials **1a–1h** (see Table S2† in ESI). The LUMO energy values of **1a–1h** were from −2.39 to −2.19 eV; very similar to the EA values. The HOMO–LUMO energy differences (energy band gaps, calculated E_g^{cal}) are presented in Table 2. The results suggest that

Table 3 Absorption spectral data and fluorescence emission spectral data for the 1,5-naphthyridines **1a–1h** in different solvents

	λ_{abs} (nm)					λ_{em} [c] (nm)				
Compd.	Tol[a]	CH_2Cl_2	THF	MeCN[b]	DMF	Tol	CH_2Cl_2	THF	MeCN	DMF
1a	304	302	303	299	303	441	448	444	450	441
1b	314	308	313	305	315	443	441	439	440	433
1c	300	294	296	292	296	345	349, 443	371, 450	346, 451	344, 440
1d	322	320	323	318	321	435	434	437	436	435
1e	319	317	318	315	318	440	439	441	441	436
1f	282, 344	275, 343	274, 342	274, 336	275, 343	434	435	434	433	441
1g	292, 342	293, 342	293, 341	292, 341	293, 342	363, 432	376, 479	373, 459	376, 515	399, 518
1h	301, 398	302, 399	297, 396	295, 389	298, 395	464	522	506	541	534

[a] Recorded in 5×10^{-5} M solutions of toluene at r.t. [b] Recorded in 5×10^{-5} M solutions of acetonitrile at r.t. [c] Recorded in $\sim 10^{-6}$ M in different solvents at rt ($\lambda_{excitation} = \lambda_{abs}$).

Table 4 Reduction cyclic voltammograms and oxidation cyclic voltammograms of compounds **1a** and **1h** (10^{-4} mol L^{-1}) in CH_2Cl_2–acetonitrile (7 : 3 v/v), TBAP (0.1 M), Scan rate = 100 mV s^{-1}

Compd.	Reduction cyclic voltammograms	Oxidation cyclic voltammograms
1a	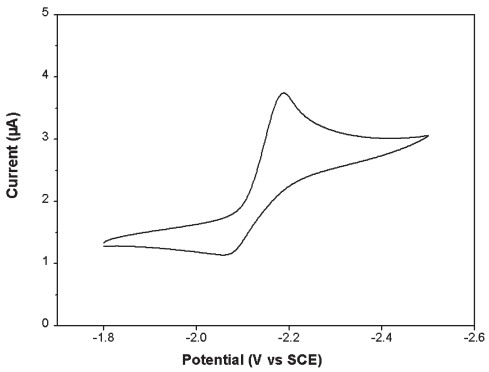	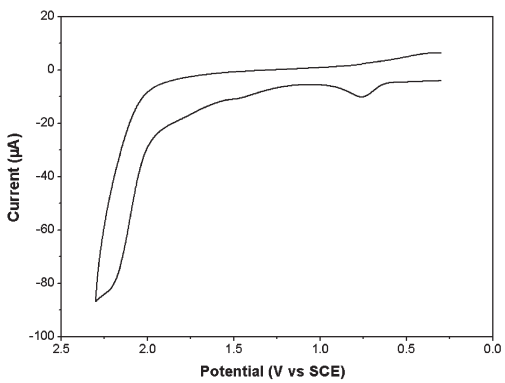
1h	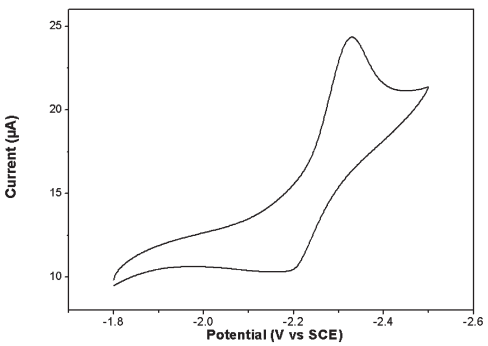	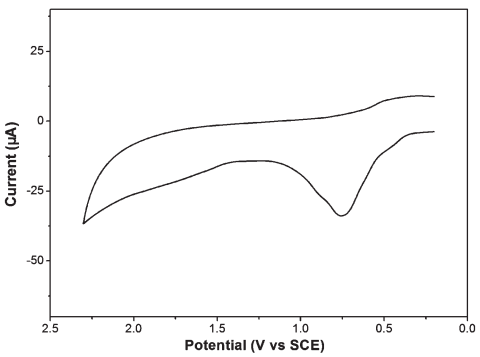

E_g^{cal} values decrease as the length of the π-conjugated system increases. These predicted E_g^{cal} values (3.09–4.32 eV) are larger than E_g^{opt} (2.77–3.79 eV) estimated from the onset of UV-vis absorption. Material **1c** has the highest E_g^{cal} and E_g^{opt} of 4.32 and 3.79 eV, respectively, whereas material **1h** with the longest conjugated length has the lowest E_g^{cal} and E_g^{opt} of 3.09 and 2.77 eV. There are factors which may be responsible for errors because the orbital energy difference between HOMO and LUMO is still an approximate estimation of the transition energy since the transition energy also contains significant contributions from some two-electron integrals. The real situation is that an accurate description of the lowest singlet excited state requires a linear combination of a number of excited configurations.

Conclusions

We have synthesized and investigated the thermal stabilities, electrochemical and photophysical properties of a series of eight novel n-type organic optoelectronic materials **1a–1h** based on a 1,5-naphthyridine core. The new materials have good solubility, therefore they have the potential to be applied as solution-processable organic layers in OLEDs. Besides, the new 4,8-substituted 1,5-naphthyridines have robust thermal stability with high glass transition temperatures. They emitted in the blue region from 400–501 nm in solid state. Additionally, the molecular design of the new multifunctional materials 1,5-naphthyridines enabled achievement of EA values (2.38–2.72 eV, below vacuum)

Table 5 Electrochemical properties[a] and energy values theoretically calculated for molecules in gas phase of 1,5-naphthyridines **1a–1h**

				E_{ox}^{peak} (V)					Calc.[c]	
Compd.	E_{red}^{peak} (V)	E_{red}^{onset} (V)	EA[b] (eV)	E_2	E_1	E_{ox}^{onset} (V)	IP[b] (eV)	E_g^{el} (eV)	LUMO (eV)	HOMO (eV)
1a	−2.10	−1.96	2.44	—	0.75	0.61	5.01	2.40	−2.29	−6.51
1b	−2.22	−2.02	2.38	2.11	0.78	0.63	5.03	2.65	−2.24	−6.32
1c	−2.01	−1.76	2.64	—	0.89	0.64	5.04	2.40	−2.52	−6.84
1d	−2.17	−2.00	2.40	1.31	0.78	0.63	5.03	2.63	−2.19	−6.08
1e	−2.14	−1.95	2.45	1.68	0.75	0.60	5.00	2.55	−2.25	−6.16
1f	−2.23	−1.96	2.44	1.27	0.77	0.61	5.01	2.57	−2.30	−5.93
1g	−2.03	−1.68	2.72	1.72	0.77	0.62	5.02	2.30	−2.39	−5.75
1h	−2.14	−1.78	2.57	—	0.74	0.49	4.89	2.27	−2.24	−5.33

[a] Redox potential recorded in dichloromethane–acetonitrile (7 : 3 v/v) solution (10^{-4} M) with 0.1 M TBAP as supporting electrolyte; scan rate = 100 mV s^{-1}, measured *versus* SCE. [b] Estimated from onset reduction/oxidation voltages with reference to SCE (4.4 eV *vs.* vacuum). [c] Optimized using density functional theory (DFT) method at the B3LYP/6-31G* level.

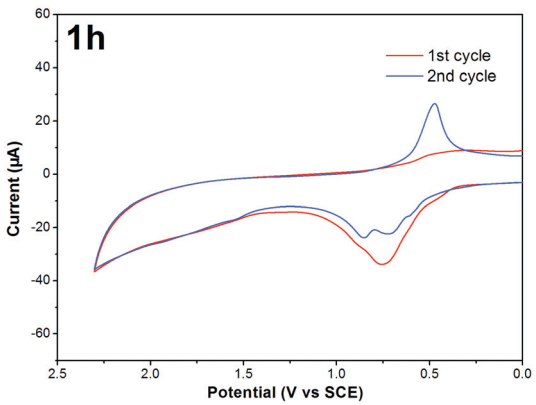

Fig. 7 Oxidation cyclic voltammograms of compound **1h** (10^{-4} mol L^{-1}) in CH_2Cl_2–acetonitrile (7 : 3 v/v), TBAP (0.1 M), scan rate = 100 mV s^{-1}; first two cycles of oxidation have been shown: polymerisation starts at the 2nd cycle.

suitable for electron-transport materials and IP values (4.89–5.04 eV, below vacuum) that could also facilitate excellent hole-injecting/hole-transport materials properties. Quantum chemical calculations using DFT B3LYP/6-31G* showed nearly identical the lowest unoccupied molecular orbitals (LUMO) of −2.39 to −2.19 eV and the highest occupied molecular orbitals (HOMO) of −5.33 to −6.84 eV. These results suggest that the 4,8-substituted 1,5-naphthyridines **1a–1g** might be promising blue-emitting (or blue-green-emitting for **1h**) materials, electron-transport materials and hole-injecting/hole-transport materials for applications in developing high-efficiency OLEDs with a simple architecture. Furthermore, we will investigate their electroluminescence and improve the device performance with these 1,5-naphthyridines as the hole-injection/hole-transport/light-emitting layer/electron-transport layer from solution processing.

References

1 J. H. Burroughes, D. D. C. Bradley, A. R. Brown, R. N. Marks, K. Mackay, R. H. Friend, P. L. Burn and A. B. Holmes, *Nature*, 1990, **347**, 539.
2 R. H. Friend, R. W. Gymer, A. B. Holmes, J. H. Burroughes, R. N. Marks, C. Taliani, D. D. C. Bradley, D. A. D. Santos, J. L. Brédas, M. Lögdlund and W. R. Salaneck, *Nature*, 1999, **397**, 121.
3 C. W. Tang and S. A. VanSlyke, *Appl. Phys. Lett.*, 1987, **51**, 913.
4 R. M. Adhikari, K. C. Anyaogu, D. C. Neckers and B. K. Shah, *J. Nanosci. Nanotechnol.*, 2010, **10**, 8004.
5 K. T. Kamtekar, A. P. Monkman and M. R. Bryce, *Adv. Mater.*, 2011, **22**, 572.
6 H. Y. Cho, E. J. Park, J.-h. Kim and L. S. Park, *J. Nanosci. Nanotechnol.*, 2008, **8**, 4916.
7 H. Park, J. Lee, I. Kang, H. Y. Chu, J.-I. Lee, S.-K. Kwon and Y.-H. Kim, *J. Mater. Chem.*, 2012, **22**, 2695.
8 T. Fuhrmann and J. Salbeck, *MRS Bull.*, 2003, **28**, 354.
9 L. S. Hung and C. H. Chen, *Mater. Sci. Eng.: R: Reports*, 2002, **39**, 143.
10 S. Kim, H. J. Kwon, S. Lee, H. Shim, Y. Chun, W. Choi, J. Kwack, D. Han, M. Song, S. Kim, S. Mohammadi, I. Kee and S. Y. Lee, *Adv. Mater.*, 2011, **23**, 3511.
11 K. A. N. Upamali, L. A. Estrada, P. K. De, X. Cai, J. A. Krause and D. C. Neekers, *Langmuir*, 2011, **27**, 1573.
12 Y.-L. Liao, C.-Y. Lin, Y.-H. Liu, K.-T. Wong, W.-Y. Hung and W.-J. Chen, *Chem. Commun.*, 2007, 1831.
13 C.-T. Chen, *Chem. Mater.*, 2004, **16**, 4389.
14 M. T. Lee, C. H. Liao, C. H. Tsai and C. H. Chen, *Adv. Mater.*, 2005, **17**, 2493.
15 I.-H. Lee and M.-S. Gong, *Bull. Korean Chem. Soc.*, 2011, **32**, 1475.
16 J.-H. Jou, W.-B. Wang, S.-Z. Chen, J.-J. Shyue, M.-F. Hsu, C.-W. Lin, S.-M. Shen, C.-J. Wang, C.-P. Liu, C.-T. Chen, M.-F. Wu and S.-W. Liu, *J. Mater. Chem.*, 2010, **20**, 8411.
17 J. K. Park, K. H. Lee, J. S. Park, J. H. Seo, Y. K. Kim and S. S. Yoon, *J. Nanosci. Nanotechnol.*, 2011, **11**, 4357.
18 R. Q. Ma, R. Hewitt, K. Rajan, J. Silvernail, K. Urbanik, M. Hack and J. J. Brown, *J. Soc. Inf. Display*, 2008, **16**, 169.
19 H. Aziz, Z. D. Popovic, N.-X. Hu, A.-M. Hor and G. Xu, *Science*, 1999, **283**, 1900.
20 Z. Li, Z. Wu, B. Jiao, P. Liu, D. Wang and X. Hou, *Chem. Phys. Lett.*, 2012, **527**, 36.
21 M. S. Park and J. Y. Lee, *Chem. Mater.*, 2011, **23**, 4338.
22 E. Ahmed, T. Earmme and S. A. Jenekhe, *Adv. Funct. Mater.*, 2011, **21**, 3889.
23 Y.-J. Li, H. Sasabe, S.-J. Su, D. Tanaka, T. Takeda, Y.-J. Pu and J. Kido, *Chem. Lett.*, 2010, **39**, 140.
24 A. K. Agrawal and S. A. Jenekhe, *Chem. Mater.*, 1996, **8**, 579.
25 J. Sanetra, D. Bogdal, M. Warzala and A. Boron, *Chem. Mater.*, 2002, **14**, 89.
26 S. Wang, Y. Q. Liu, X. W. Zhan, G. Yu and D. B. Zhu, *Synth. Met.*, 2003, **137**, 1153.
27 B. M. Bahirwar, R. G. Atram, R. B. Pode and S. V. Moharil, *Mater. Chem. Phys.*, 2007, **106**, 364.
28 K. W. Song, J. Y. Lee, S. W. Heo and D. K. Moon, *J. Nanosci. Nanotechnol.*, 2010, **10**, 99.
29 K. Ono, Y. Okazaki, M. Ohkita, K. Saito and Y. Yamashita, *Heterocycles*, 2004, **63**, 2207.
30 P. Karastatiris, J. A. Mikroyannidis, I. K. Spiliopoulos, A. P. Kulkarni and S. A. Jenekhe, *Macromolecules*, 2004, **37**, 7867.
31 A. P. Kulkarni, Y. Zhu and S. A. Jenekhe, *Macromolecules*, 2005, **38**, 1553.

32 L. Ying, J. Zou, W. Yang, A. Zhang, Z. Wu, W. Zhao and Y. Cao, *Dyes Pigm.*, 2009, **82**, 251.
33 H. Wang, G. Chen, Y. Liu, L. Hu, X. Xu and S. Ji, *Dyes Pigm.*, 2009, **83**, 269.
34 S. Liu, P. Jiang, G. Song, R. Liu and H. Zhu, *Dyes Pigm.*, 2009, **81**, 218.
35 S. Liu, Q. Wang, P. Jiang, R. Liu, G. Song, H. Zhu and S.-W. Yang, *Dyes Pigm.*, 2010, **85**, 51.
36 Q. Zhang, P. Jiang, K. Wang, G. Song and H. Zhu, *Dyes Pigm.*, 2011, **91**, 89.
37 C. J. Tonzola, M. M. Alam, W. Kaminsky and S. A. Jenekhe, *J. Am. Chem. Soc.*, 2003, **125**, 13548.
38 T. W. Kwon, M. M. Alam and S. A. Jenekhe, *Chem. Mater.*, 2004, **16**, 4657.
39 E. Moreno, S. Perez-Silanes, S. Gouravaram, A. Macharam, S. Ancizu, E. Torres, I. Aldana, A. Monge and P. W. Crawford, *Electrochim. Acta*, 2011, **56**, 3270.
40 M. S. Liu, Y. Liu, R. Craig Urian, H. Ma and A. K.-Y. Jen, *J. Mater. Chem.*, 1999, **9**, 2201.
41 J. E. Anthony, A. Facchetti, M. Heeney, S. R. Marder and X. Zhan, *Adv. Mater.*, 2010, **22**, 3876.
42 S.-H. Liao, J.-R. Shiu, S.-W. Liu, S.-J. Yeh, Y.-H. Chen, C.-T. Chen, T. J. Chow and C.-I. Wu, *J. Am. Chem. Soc.*, 2009, **131**, 763.
43 K. W. Chen Chen, P. Jiang, G. Song and H. Zhu, *Inorg. Chem. Commun.*, 2012, **17**, 116.
44 A. N. Singh and R. P. Thummel, *Inorg. Chem.*, 2009, **48**, 6459.
45 S. Tao, Y. Jiang, S.-L. Lai, M.-K. Fung, Y. Zhou, X. Zhang, W. Zhao and C.-S. Lee, *Org. Electron.*, 2011, **12**, 358.
46 L. Chen, J. Ding, Y. Cheng, Z. Xie, L. Wang, X. Jing and F. Wang, *Chem.–Asian J.*, 2011, **6**, 1372.
47 A. Chaskar, H.-F. Chen and K.-T. Wong, *Adv. Mater.*, 2011, **23**, 3876.
48 J. Ding, Q. Wang, L. Zhao, D. Ma, L. Wang, X. Jing and F. Wang, *J. Mater. Chem.*, 2010, **20**, 8126.
49 S. Tao, L. Li, J. Yu, Y. Jiang, Y. Zhou, C.-S. Lee, S.-T. Lee, X. Zhang and O. Kwon, *Chem. Mater.*, 2009, **21**, 1284.
50 A. Kraft, A. C. Grimsdale and A. B. Holmes, *Angew. Chem., Int. Ed.*, 1998, **37**, 402.
51 S. B. Brown and M. J. S. Dewar, *J. Org. Chem.*, 1978, **43**, 1331.
52 R. T. Hawkins, W. J. Lennarz and H. R. Snyder, *J. Am. Chem. Soc.*, 1960, **82**, 3053.
53 W. Z. Yuan, P. Lu, S. Chen, J. W. Y. Lam, Z. Wang, Y. Liu, H. S. Kwok, Y. Ma and B. Z. Tang, *Adv. Mater.*, 2010, **22**, 2159.
54 W. Wu, C. Cheng, W. Wu, H. Guo, S. Ji, P. Song, K. Han, J. Zhao, X. Zhang, Y. Wu and G. Du, *Eur. J. Inorg. Chem.*, 2010, **2010**, 4683.
55 H.-P. Shi, L. Xu, Y. Cheng, J.-Y. He, J.-X. Dai, L.-W. Xing, B.-Q. Chen and L. Fang, *Spectrochim. Acta, Part A*, 2011, **81**, 730.
56 M.-k. Leung, M.-Y. Chou, Y. O. Su, C. L. Chiang, H.-L. Chen, C. F. Yang, C.-C. Yang, C.-C. Lin and H.-T. Chen, *Org. Lett.*, 2003, **5**, 839.
57 K. Tanemura, T. Suzuki, Y. Nishida, K. Satsumabayashi and T. Horaguchiy, *Chem. Lett.*, 2003, **32**, 932.
58 G. M. Sheldrick, *SHELXL-97. Program for the Refinement of Crystal Structures*, University of Göttingen, Germany, 1997.
59 P. Singh, A. Baheti and K. R. J. Thomas, *J. Org. Chem.*, 2011, **76**, 6134.
60 P. Tyagi, A. Venkateswararao and K. R. J. Thomas, *J. Org. Chem.*, 2011, **76**, 4571.
61 M. Ananth Reddy, A. Thomas, G. Mallesham, B. Sridhar, V. Jayathirtha Rao and K. Bhanuprakash, *Tetrahedron Lett.*, 2011, **52**, 6942.
62 Y. Tao, Q. Wang, C. Yang, C. Zhong, K. Zhang, J. Qin and D. Ma, *Adv. Funct. Mater.*, 2010, **20**, 304.
63 A. L. Fisher, K. E. Linton, K. T. Kamtekar, C. Pearson, M. R. Bryce and M. C. Petty, *Chem. Mater.*, 2011, **23**, 1640.
64 S. A. Jenekhe, L. Lu and M. M. Alam, *Macromolecules*, 2001, **34**, 7315.
65 H. Li, A. S. Batsanov, K. C. Moss, H. L. Vaughan, F. B. Dias, K. T. Kamtekar, M. R. Bryce and A. P. Monkman, *Chem. Commun.*, 2010, **46**, 4812.
66 C. J. Tonzola, A. P. Kulkarni, A. P. Gifford, W. Kaminsky and S. A. Jenekhe, *Adv. Funct. Mater.*, 2007, **17**, 863.
67 E. Ahmed, T. Earmme and S. A. Jenekhe, *Adv. Funct. Mater.*, 2011, **21**, 3889.
68 C. J. Tonzola, M. M. Alam, B. A. Bean and S. A. Jenekhe, *Macromolecules*, 2004, **37**, 3554.
69 C. J. Tonzola, M. M. Alam and S. A. Jenekhe, *Macromolecules*, 2005, **38**, 9539.
70 X. Zhang, D. M. Kale and S. A. Jenekhe, *Macromolecules*, 2001, **35**, 382.
71 K. T. Kamtekar, C. Wang, S. Bettington, A. S. Batsanov, I. F. Perepichka, M. R. Bryce, J. H. Ahn, M. Rabinal and M. C. Petty, *J. Mater. Chem.*, 2006, **16**, 3823.
72 H.-P. Lin, F. Zhou, X.-W. Zhang, D.-B. Yu, J. Li, L. Zhang, X.-Y. Jiang and Z.-L. Zhang, *Curr. Appl. Phys.*, 2011, **11**, 853.
73 H. H. Fong, A. Papadimitratos, J. Hwang, A. Kahn and G. G. Malliaras, *Adv. Funct. Mater.*, 2009, **19**, 304.
74 K. R. Choudhury, J. Lee, N. Chopra, A. Gupta, X. Jiang, F. Amy and F. So, *Adv. Funct. Mater.*, 2009, **19**, 491.
75 Z. H. Li, M. S. Wong, Y. Tao and J. Lu, *Chem.–Eur. J.*, 2005, **11**, 3285.

